

# **Tau Lepton Production in $ep$ Collisions at HERA**

H1 Collaboration

## **Abstract**

The production of tau leptons in  $ep$  collisions is investigated using data recorded by the H1 detector at HERA in the period 1994-2000. Tau leptons are identified by detecting their decay products, using leptonic and hadronic decay modes. The cross section for the production of tau lepton pairs is measured for the first time at HERA. Furthermore, a search for events with an energetic isolated tau lepton and with large missing transverse momentum is performed. The results are found to be in agreement with the Standard Model predictions.

Submitted to Eur. Phys. J. C

A. Aktas<sup>9</sup>, V. Andreev<sup>25</sup>, T. Anthonis<sup>3</sup>, B. Antunovic<sup>26</sup>, S. Aplin<sup>9</sup>, A. Asmone<sup>33</sup>,  
 A. Astvatsatourov<sup>3</sup>, A. Babaev<sup>24,†</sup>, S. Backovic<sup>30</sup>, A. Baghdasaryan<sup>37</sup>, P. Baranov<sup>25</sup>, E. Barrelet<sup>29</sup>,  
 W. Bartel<sup>9</sup>, S. Baudrand<sup>27</sup>, S. Baumgartner<sup>39</sup>, J. Becker<sup>40</sup>, M. Beckingham<sup>9</sup>, O. Behnke<sup>12</sup>,  
 O. Behrendt<sup>6</sup>, A. Belousov<sup>25</sup>, N. Berger<sup>39</sup>, J.C. Bizot<sup>27</sup>, M.-O. Boenig<sup>6</sup>, V. Boudry<sup>28</sup>, J. Bracinik<sup>26</sup>,  
 G. Brandt<sup>12</sup>, V. Brisson<sup>27</sup>, D. Bruncko<sup>15</sup>, F.W. Büsser<sup>10</sup>, A. Bunyatyan<sup>11,37</sup>, G. Buschhorn<sup>26</sup>,  
 L. Bystritskaya<sup>24</sup>, A.J. Campbell<sup>9</sup>, F. Cassol-Brunner<sup>21</sup>, K. Cerny<sup>32</sup>, V. Cerny<sup>15,46</sup>, V. Chekelian<sup>26</sup>,  
 J.G. Contreras<sup>22</sup>, J.A. Coughlan<sup>4</sup>, B.E. Cox<sup>20</sup>, G. Cozzika<sup>8</sup>, J. Cvach<sup>31</sup>, J.B. Dainton<sup>17</sup>, W.D. Dau<sup>14</sup>,  
 K. Daum<sup>36,42</sup>, Y. de Boer<sup>24</sup>, B. Delcourt<sup>27</sup>, M. Del Degan<sup>39</sup>, A. De Roeck<sup>9,44</sup>, E.A. De Wolf<sup>3</sup>,  
 C. Diaconu<sup>21</sup>, V. Dodonov<sup>11</sup>, A. Dubak<sup>30,45</sup>, G. Eckerlin<sup>9</sup>, V. Efremenko<sup>24</sup>, S. Egli<sup>35</sup>, R. Eichler<sup>35</sup>,  
 F. Eisele<sup>12</sup>, A. Eliseev<sup>25</sup>, E. Elsen<sup>9</sup>, S. Essenov<sup>24</sup>, A. Falkewicz<sup>5</sup>, P.J.W. Faulkner<sup>2</sup>, L. Favart<sup>3</sup>,  
 A. Fedotov<sup>24</sup>, R. Felst<sup>9</sup>, J. Feltesse<sup>8</sup>, J. Ferencei<sup>15</sup>, L. Finke<sup>10</sup>, M. Fleischer<sup>9</sup>, G. Flucke<sup>33</sup>,  
 A. Fomenko<sup>25</sup>, G. Franke<sup>9</sup>, T. Frisson<sup>28</sup>, E. Gabathuler<sup>17</sup>, E. Garutti<sup>9</sup>, J. Gayler<sup>9</sup>, C. Gerlich<sup>12</sup>,  
 S. Ghazaryan<sup>37</sup>, S. Ginzburgskaya<sup>24</sup>, A. Glazov<sup>9</sup>, I. Glushkov<sup>38</sup>, L. Goerlich<sup>5</sup>, M. Goettlich<sup>9</sup>,  
 N. Gogitidze<sup>25</sup>, S. Gorbounov<sup>38</sup>, C. Grab<sup>39</sup>, T. Greenshaw<sup>17</sup>, M. Gregori<sup>18</sup>, B.R. Grell<sup>9</sup>,  
 G. Grindhammer<sup>26</sup>, C. Gwilliam<sup>20</sup>, D. Haidt<sup>9</sup>, L. Hajduk<sup>5</sup>, M. Hansson<sup>19</sup>, G. Heinzelmann<sup>10</sup>,  
 R.C.W. Henderson<sup>16</sup>, H. Henschel<sup>38</sup>, G. Herrera<sup>23</sup>, M. Hildebrandt<sup>35</sup>, K.H. Hiller<sup>38</sup>, D. Hoffmann<sup>21</sup>,  
 R. Horisberger<sup>35</sup>, A. Hovhannisyanyan<sup>37</sup>, T. Hreus<sup>3,43</sup>, S. Hussain<sup>18</sup>, M. Ibbotson<sup>20</sup>, M. Ismail<sup>20</sup>,  
 M. Jaquet<sup>27</sup>, L. Janauschek<sup>26</sup>, X. Janssen<sup>3</sup>, V. Jemanov<sup>10</sup>, L. Jönsson<sup>19</sup>, D.P. Johnson<sup>3</sup>, A.W. Jung<sup>13</sup>,  
 H. Jung<sup>19,9</sup>, M. Kapichine<sup>7</sup>, J. Katzy<sup>9</sup>, I.R. Kenyon<sup>2</sup>, C. Kiesling<sup>26</sup>, M. Klein<sup>38</sup>, C. Kleinwort<sup>9</sup>,  
 T. Klimkovich<sup>9</sup>, T. Kluge<sup>9</sup>, G. Knies<sup>9</sup>, A. Knutsson<sup>19</sup>, V. Korbel<sup>9</sup>, P. Kostka<sup>38</sup>, K. Krastev<sup>9</sup>,  
 J. Kretschmar<sup>38</sup>, A. Kropivnitskaya<sup>24</sup>, K. Krüger<sup>13</sup>, M.P.J. Landon<sup>18</sup>, W. Lange<sup>38</sup>,  
 G. Laštovička-Medin<sup>30</sup>, P. Laycock<sup>17</sup>, A. Lebedev<sup>25</sup>, G. Leibenguth<sup>39</sup>, V. Lendermann<sup>13</sup>,  
 S. Levonian<sup>9</sup>, L. Lindfeld<sup>40</sup>, K. Lipka<sup>38</sup>, A. Liptaj<sup>26</sup>, B. List<sup>39</sup>, J. List<sup>10</sup>, E. Lobodzinska<sup>38,5</sup>,  
 N. Loktionova<sup>25</sup>, R. Lopez-Fernandez<sup>23</sup>, V. Lubimov<sup>24</sup>, A.-I. Lucaci-Timoce<sup>9</sup>, H. Lueders<sup>10</sup>,  
 D. Lüke<sup>6,9</sup>, T. Lux<sup>10</sup>, L. Lytkin<sup>11</sup>, A. Makankine<sup>7</sup>, N. Malden<sup>20</sup>, E. Malinovski<sup>25</sup>, S. Mangano<sup>39</sup>,  
 P. Marage<sup>3</sup>, R. Marshall<sup>20</sup>, L. Marti<sup>9</sup>, M. Martisikova<sup>9</sup>, H.-U. Martyn<sup>1</sup>, S.J. Maxfield<sup>17</sup>, A. Mehta<sup>17</sup>,  
 K. Meier<sup>13</sup>, A.B. Meyer<sup>9</sup>, H. Meyer<sup>36</sup>, J. Meyer<sup>9</sup>, V. Michels<sup>9</sup>, S. Mikocki<sup>5</sup>, I. Milcewicz-  
 Mika<sup>5</sup>, D. Milstead<sup>17</sup>, D. Mladenov<sup>34</sup>, A. Mohamed<sup>17</sup>, F. Moreau<sup>28</sup>, A. Morozov<sup>7</sup>, J.V. Morris<sup>4</sup>,  
 M.U. Mozer<sup>12</sup>, K. Müller<sup>40</sup>, P. Murín<sup>15,43</sup>, K. Nankov<sup>34</sup>, B. Naroska<sup>10</sup>, Th. Naumann<sup>38</sup>,  
 P.R. Newman<sup>2</sup>, C. Niebuhr<sup>9</sup>, A. Nikiforov<sup>26</sup>, G. Nowak<sup>5</sup>, K. Nowak<sup>40</sup>, M. Nozicka<sup>32</sup>,  
 R. Oganezov<sup>37</sup>, B. Olivier<sup>26</sup>, J.E. Olsson<sup>9</sup>, S. Osman<sup>19</sup>, D. Ozerov<sup>24</sup>, V. Palichik<sup>7</sup>, I. Panagoulas<sup>9</sup>,  
 T. Papadopoulou<sup>9</sup>, C. Pascaud<sup>27</sup>, G.D. Patel<sup>17</sup>, H. Peng<sup>9</sup>, E. Perez<sup>8</sup>, D. Perez-Astudillo<sup>22</sup>,  
 A. Perieanu<sup>9</sup>, A. Petrukhin<sup>24</sup>, D. Pitzl<sup>9</sup>, R. Plačákytė<sup>26</sup>, B. Porthault<sup>27</sup>, B. Povh<sup>11</sup>, P. Prideaux<sup>17</sup>,  
 A.J. Rahmat<sup>17</sup>, N. Raicevic<sup>30</sup>, P. Reimer<sup>31</sup>, A. Rimmer<sup>17</sup>, C. Risler<sup>9</sup>, E. Rizvi<sup>18</sup>, P. Robmann<sup>40</sup>,  
 B. Roland<sup>3</sup>, R. Roosen<sup>3</sup>, A. Rostovtsev<sup>24</sup>, Z. Rurikova<sup>26</sup>, S. Rusakov<sup>25</sup>, F. Salvaire<sup>10</sup>,  
 D.P.C. Sankey<sup>4</sup>, E. Sauvan<sup>21</sup>, S. Schätzel<sup>9</sup>, S. Schmidt<sup>9</sup>, S. Schmitt<sup>9</sup>, C. Schmitz<sup>40</sup>, L. Schoeffel<sup>8</sup>,  
 A. Schöning<sup>39</sup>, H.-C. Schultz-Coulon<sup>13</sup>, F. Sefkow<sup>9</sup>, R.N. Shaw-West<sup>2</sup>, I. Sheviakov<sup>25</sup>,  
 L.N. Shtarkov<sup>25</sup>, T. Sloan<sup>16</sup>, P. Smirnov<sup>25</sup>, Y. Soloviev<sup>25</sup>, D. South<sup>9</sup>, V. Spaskov<sup>7</sup>, A. Specka<sup>28</sup>,  
 M. Steder<sup>9</sup>, B. Stella<sup>33</sup>, J. Stiewe<sup>13</sup>, A. Stoilov<sup>34</sup>, U. Straumann<sup>40</sup>, D. Sunar<sup>3</sup>, V. Tchoulakov<sup>7</sup>,  
 G. Thompson<sup>18</sup>, P.D. Thompson<sup>2</sup>, T. Toll<sup>9</sup>, F. Tomasz<sup>15</sup>, D. Traynor<sup>18</sup>, P. Truöl<sup>40</sup>, I. Tsakov<sup>34</sup>,  
 G. Tsipolitis<sup>9,41</sup>, I. Tsurin<sup>9</sup>, J. Turnau<sup>5</sup>, E. Tzamariudaki<sup>26</sup>, K. Urban<sup>13</sup>, M. Urban<sup>40</sup>, A. Usik<sup>25</sup>,  
 D. Utkin<sup>24</sup>, A. Valkárová<sup>32</sup>, C. Vallée<sup>21</sup>, P. Van Mechelen<sup>3</sup>, A. Vargas Trevino<sup>6</sup>, Y. Vazdik<sup>25</sup>,  
 C. Veelken<sup>17</sup>, S. Vinokurova<sup>9</sup>, V. Volchinski<sup>37</sup>, K. Wacker<sup>6</sup>, G. Weber<sup>10</sup>, R. Weber<sup>39</sup>, D. Wegener<sup>6</sup>,  
 C. Werner<sup>12</sup>, M. Wessels<sup>9</sup>, B. Wessling<sup>9</sup>, Ch. Wissing<sup>6</sup>, R. Wolf<sup>12</sup>, E. Wunsch<sup>9</sup>, S. Xella<sup>40</sup>,  
 W. Yan<sup>9</sup>, V. Yeganov<sup>37</sup>, J. Žáček<sup>32</sup>, J. Zálešák<sup>31</sup>, Z. Zhang<sup>27</sup>, A. Zhelezov<sup>24</sup>, A. Zhokin<sup>24</sup>,  
 Y.C. Zhu<sup>9</sup>, J. Zimmermann<sup>26</sup>, T. Zimmermann<sup>39</sup>, H. Zohrabyan<sup>37</sup>, and F. Zomer<sup>27</sup>

- <sup>1</sup> *I. Physikalisches Institut der RWTH, Aachen, Germany<sup>a</sup>*
- <sup>2</sup> *School of Physics and Astronomy, University of Birmingham, Birmingham, UK<sup>b</sup>*
- <sup>3</sup> *Inter-University Institute for High Energies ULB-VUB, Brussels; Universiteit Antwerpen, Antwerpen; Belgium<sup>c</sup>*
- <sup>4</sup> *Rutherford Appleton Laboratory, Chilton, Didcot, UK<sup>b</sup>*
- <sup>5</sup> *Institute for Nuclear Physics, Cracow, Poland<sup>d</sup>*
- <sup>6</sup> *Institut für Physik, Universität Dortmund, Dortmund, Germany<sup>a</sup>*
- <sup>7</sup> *Joint Institute for Nuclear Research, Dubna, Russia*
- <sup>8</sup> *CEA, DSM/DAPNIA, CE-Saclay, Gif-sur-Yvette, France*
- <sup>9</sup> *DESY, Hamburg, Germany*
- <sup>10</sup> *Institut für Experimentalphysik, Universität Hamburg, Hamburg, Germany<sup>a</sup>*
- <sup>11</sup> *Max-Planck-Institut für Kernphysik, Heidelberg, Germany*
- <sup>12</sup> *Physikalisches Institut, Universität Heidelberg, Heidelberg, Germany<sup>a</sup>*
- <sup>13</sup> *Kirchhoff-Institut für Physik, Universität Heidelberg, Heidelberg, Germany<sup>a</sup>*
- <sup>14</sup> *Institut für Experimentelle und Angewandte Physik, Universität Kiel, Kiel, Germany*
- <sup>15</sup> *Institute of Experimental Physics, Slovak Academy of Sciences, Košice, Slovak Republic<sup>f</sup>*
- <sup>16</sup> *Department of Physics, University of Lancaster, Lancaster, UK<sup>b</sup>*
- <sup>17</sup> *Department of Physics, University of Liverpool, Liverpool, UK<sup>b</sup>*
- <sup>18</sup> *Queen Mary and Westfield College, London, UK<sup>b</sup>*
- <sup>19</sup> *Physics Department, University of Lund, Lund, Sweden<sup>g</sup>*
- <sup>20</sup> *Physics Department, University of Manchester, Manchester, UK<sup>b</sup>*
- <sup>21</sup> *CPPM, CNRS/IN2P3 - Univ. Mediterranee, Marseille - France*
- <sup>22</sup> *Departamento de Física Aplicada, CINVESTAV, Mérida, Yucatán, México<sup>j</sup>*
- <sup>23</sup> *Departamento de Física, CINVESTAV, México<sup>j</sup>*
- <sup>24</sup> *Institute for Theoretical and Experimental Physics, Moscow, Russia<sup>k</sup>*
- <sup>25</sup> *Lebedev Physical Institute, Moscow, Russia<sup>e</sup>*
- <sup>26</sup> *Max-Planck-Institut für Physik, München, Germany*
- <sup>27</sup> *LAL, Université de Paris-Sud 11, IN2P3-CNRS, Orsay, France*
- <sup>28</sup> *LLR, Ecole Polytechnique, IN2P3-CNRS, Palaiseau, France*
- <sup>29</sup> *LPNHE, Universités Paris VI and VII, IN2P3-CNRS, Paris, France*
- <sup>30</sup> *Faculty of Science, University of Montenegro, Podgorica, Serbia and Montenegro<sup>e</sup>*
- <sup>31</sup> *Institute of Physics, Academy of Sciences of the Czech Republic, Praha, Czech Republic<sup>h</sup>*
- <sup>32</sup> *Faculty of Mathematics and Physics, Charles University, Praha, Czech Republic<sup>h</sup>*
- <sup>33</sup> *Dipartimento di Fisica Università di Roma Tre and INFN Roma 3, Roma, Italy*
- <sup>34</sup> *Institute for Nuclear Research and Nuclear Energy, Sofia, Bulgaria<sup>e</sup>*
- <sup>35</sup> *Paul Scherrer Institut, Villigen, Switzerland*
- <sup>36</sup> *Fachbereich C, Universität Wuppertal, Wuppertal, Germany*
- <sup>37</sup> *Yerevan Physics Institute, Yerevan, Armenia*
- <sup>38</sup> *DESY, Zeuthen, Germany*
- <sup>39</sup> *Institut für Teilchenphysik, ETH, Zürich, Switzerland<sup>i</sup>*
- <sup>40</sup> *Physik-Institut der Universität Zürich, Zürich, Switzerland<sup>i</sup>*
  
- <sup>41</sup> *Also at Physics Department, National Technical University, Zografou Campus, GR-15773 Athens, Greece*
- <sup>42</sup> *Also at Rechenzentrum, Universität Wuppertal, Wuppertal, Germany*

<sup>43</sup> Also at University of P.J. Šafárik, Košice, Slovak Republic

<sup>44</sup> Also at CERN, Geneva, Switzerland

<sup>45</sup> Also at Max-Planck-Institut für Physik, München, Germany

<sup>46</sup> Also at Comenius University, Bratislava, Slovak Republic

† Deceased

<sup>a</sup> Supported by the Bundesministerium für Bildung und Forschung, FRG, under contract numbers 05 H1 1GUA /1, 05 H1 1PAA /1, 05 H1 1PAB /9, 05 H1 1PEA /6, 05 H1 1VHA /7 and 05 H1 1VHB /5

<sup>b</sup> Supported by the UK Particle Physics and Astronomy Research Council, and formerly by the UK Science and Engineering Research Council

<sup>c</sup> Supported by FNRS-FWO-Vlaanderen, IISN-IKW and IWT and by Interuniversity Attraction Poles Programme, Belgian Science Policy

<sup>d</sup> Partially Supported by the Polish State Committee for Scientific Research, SPUB/DESY/P003/DZ 118/2003/2005

<sup>e</sup> Supported by the Deutsche Forschungsgemeinschaft

<sup>f</sup> Supported by VEGA SR grant no. 2/4067/ 24

<sup>g</sup> Supported by the Swedish Natural Science Research Council

<sup>h</sup> Supported by the Ministry of Education of the Czech Republic under the projects LC527 and INGO-1P05LA259

<sup>i</sup> Supported by the Swiss National Science Foundation

<sup>j</sup> Supported by CONACYT, México, grant 400073-F

<sup>k</sup> Partially Supported by Russian Foundation for Basic Research, grants 03-02-17291 and 04-02-16445

# 1 Introduction

In the Standard Model (SM), tau leptons are produced either in pairs or in association with a tau anti-neutrino, as expected from lepton flavour conservation. In electron–proton collisions, pairs of tau leptons are produced via photon–photon interaction  $\gamma\gamma \rightarrow \tau^+\tau^-$  (figure 1a), in which a photon from the electron interacts with a photon emitted by the proton [1]. Tau leptons and tau anti-neutrinos are produced in  $W$  boson decays, as illustrated in figure 1b [2]. The signature of these events is a high transverse momentum ( $P_T$ ) isolated tau lepton, large missing transverse momentum  $P_T^{\text{miss}}$  due to the undetected neutrinos, and a hadronic system, typically of low  $P_T$ .

This paper presents a measurement of the production of tau lepton pairs ( $\tau^+\tau^-$ ) and a search for events with an isolated tau lepton accompanied by large missing transverse momentum ( $\tau + P_T^{\text{miss}}$ ). The measurement of  $\tau^+\tau^-$  production is performed at low transverse momentum considering both leptonic and hadronic tau decays. This measurement complements that of electron and muon pair production previously performed by the H1 collaboration [3, 4]. In the search for  $\tau + P_T^{\text{miss}}$  events tau decays are identified in the hadronic channel only. This search complements the previous H1 measurements of the production of events with an isolated electron or muon and large missing transverse momentum, which have revealed an excess over the SM expectation of events containing in addition a high  $P_T$  hadronic system [5–7]. The ZEUS collaboration has also studied the production of events with an isolated lepton and large missing transverse momentum [8–10].

The analysis is based on data from electron<sup>1</sup>–proton collisions at a centre-of-mass energy of 301 or 319 GeV, recorded by the H1 experiment at HERA in the period 1994–2000. The total integrated luminosity amounts to  $106 \text{ pb}^{-1}$  for the measurement of  $\tau^+\tau^-$  production and  $115 \text{ pb}^{-1}$  for the search for  $\tau + P_T^{\text{miss}}$  events.

This paper is organised as follows. The physics processes leading to tau lepton production at HERA are described in section 2 together with the relevant background processes. In section 3 the H1 detector and the experimental conditions are briefly described. Particle identification is presented in section 4. The selection of events with tau pairs and the resulting measurements are described in section 5. The search for events with an isolated high  $P_T$  tau lepton and large missing transverse momentum is presented in section 6. A summary is given in section 7.

## 2 Signal and Background Processes

The Standard Model processes leading to tau lepton production in electron–proton collisions are briefly outlined in this section, together with the dominant background processes. For each process,  $X$  is used to label the hadronic final state, excluding the tau decay products.

The following processes, denoted henceforth as signal, lead to events containing genuine tau leptons in the final state:

---

<sup>1</sup>In this paper, the name of the particle is used for both particles and anti-particles, unless otherwise stated (e.g. “electron” is used generically to refer to both electrons and positrons).

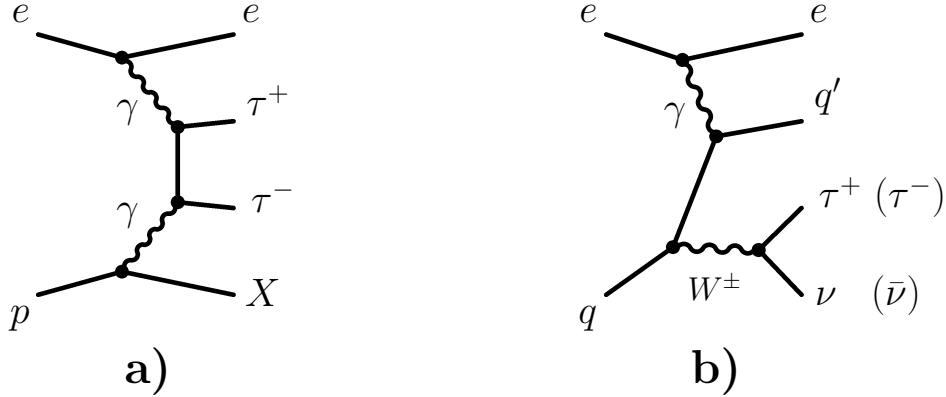


Figure 1: Diagrams of the main production mechanisms of tau leptons in electron–proton collisions: **a)** tau pair production via photon–photon collisions and **b)** single  $W$  boson production followed by the subsequent decay of the  $W$  into a tau lepton and a tau anti–neutrino.

- **Tau pair production:**  $ep \rightarrow e\tau^+\tau^-X$

The production of tau pairs proceeds mainly via photon–photon collisions [1], as shown in figure 1a. The proton can remain intact (elastic production, which dominates) or be dissociated in the interaction (inelastic production). The incident electron is usually scattered at small angles and is often not observed in the main detector. Only a small fraction of the total cross section is visible in the detector, as the cross section steeply falls with the transverse momentum  $P_T^\tau$  of the tau leptons. The cross section is about 20 pb for  $P_T^\tau > 2$  GeV. This process is modelled using the GRAPE [11] Monte Carlo (MC) generator.

- **Production of  $W$  bosons:**  $ep \rightarrow eWX \rightarrow e\tau\nu_\tau X$

The dominant production mechanism for  $W$  bosons in  $ep$  collisions [2] is depicted in figure 1b. The cross section is largest in the photoproduction regime (photon–proton collisions), in which the  $W$  boson usually has small transverse momentum and the scattered electron is not observed in the main detector. The  $W$  production cross section at HERA is about 1 pb, resulting in a cross section of about 0.1 pb for the process  $ep \rightarrow eWX \rightarrow e\tau\nu_\tau X$ . This process is modelled using the EPVEC generator [2]. The next–to–leading order QCD corrections to  $W$  production [12] are taken into account by weighting the events as a function of the rapidity and transverse momentum of the  $W$  boson [13].

The following processes, denoted henceforth as background, do not contain genuine tau leptons but contribute to the selected samples through misidentification or mismeasurement:

- **Neutral Current deep inelastic scattering (NC DIS):**  $ep \rightarrow eX$

The scattered electron, or a quark or gluon that hadronises into a collimated jet of low particle multiplicity, may fake the hadronic tau decay signature. Missing transverse momentum may occur in NC DIS events because of fluctuations in the detector response and

limited geometrical acceptance. The RAPGAP [14] generator is used to calculate this contribution to the background, including diffractive processes.

- **Photoproduction of jets:**  $\gamma p \rightarrow X$

Photoproduction processes may contribute to the background if a jet in the hadronic final state is misidentified as a hadronic tau decay. As in NC DIS events, missing transverse momentum may be measured due to fluctuations in the detector response and limited geometrical acceptance. The PYTHIA generator [15] is used to calculate the contribution from non-diffractive hard scattering photoproduction processes. The contribution from diffractive photoproduction processes is simulated using the RAPGAP generator.

- **Electron or muon pair production:**  $ep \rightarrow ee^+e^-X$  or  $e\mu^+\mu^-X$

Events with two leptons ( $ee$ ,  $\mu\mu$  or  $e\mu$ ) may mimic events containing  $\tau^+\tau^-$  pairs in which both tau leptons decay leptonically. The production of electron or muon pairs may also contribute as background if one electron or muon is not identified and fakes the signature of a hadronic tau decay. This contribution is calculated using the GRAPE generator.

- **Charged current deep inelastic scattering (CC DIS):**  $ep \rightarrow \nu X$

CC DIS events contain genuine large missing transverse momentum due to the presence of a neutrino in the final state. A jet originating from the struck quark may fake the hadronic tau decay signature. This process constitutes the main background contribution to the  $\tau + P_T^{\text{miss}}$  analysis. The DJANGO [16] generator is used to calculate the background contribution from CC DIS processes.

All generated events are passed through the full GEANT [17] based simulation of the H1 apparatus and are reconstructed using the same procedure that is applied to the data.

### 3 Experimental Conditions

At HERA, electrons of energy  $E_e = 27.6$  GeV collide with protons of energy  $E_p = 820$  or  $920$  GeV, corresponding to a centre-of-mass energy  $\sqrt{s}$  of 301 or 319 GeV, respectively. The analysed datasets consist of  $36.5 \text{ pb}^{-1}$  of  $e^+p$  collisions at  $\sqrt{s} = 301$  GeV (taken in the period 1994-1997),  $65.1 \text{ pb}^{-1}$  of  $e^+p$  collisions at  $\sqrt{s} = 319$  GeV (1999-2000) and  $13.6 \text{ pb}^{-1}$  of  $e^-p$  collisions at  $\sqrt{s} = 319$  GeV (1998-1999), corresponding to a total integrated luminosity of  $115.2 \text{ pb}^{-1}$ . The data recorded in the period 1994-1995 are not included for the measurement of tau pair production, reducing the integrated luminosity to  $106.0 \text{ pb}^{-1}$  for this analysis.

A detailed description of the H1 detector can be found in [18]. Only the components essential to the present analysis are described here. A right handed cartesian coordinate system is used with the origin at the nominal primary  $ep$  interaction vertex. The proton beam direction defines the  $z$  axis. The polar angles  $\theta$  and transverse momenta  $P_T$  of all particles are defined with respect to this axis. The azimuthal angle  $\phi$  defines the particle direction in the transverse plane. The pseudorapidity is defined as  $\eta = -\ln \tan \frac{\theta}{2}$ .

The inner tracking system contains the central ( $20^\circ < \theta < 160^\circ$ ) and forward ( $7^\circ < \theta < 25^\circ$ ) drift chambers, and the proportional chambers which are employed for triggering purposes. It

is used to determine the position of the interaction vertex and to measure the trajectories of charged particles. Particle transverse momenta and charges are determined from the curvature of the trajectories in a solenoidal magnetic field of 1.15 T.

Hadronic final state particles as well as electrons and photons are absorbed in the highly segmented liquid argon (LAr) calorimeter [19] ( $4^\circ < \theta < 154^\circ$ ) which is 20 to 30 radiation lengths deep depending on the polar angle. The hadronic section of the LAr calorimeter is 5 to 8 hadronic interaction lengths deep. Electromagnetic shower energies are measured with a precision of  $\sigma(E)/E = 12\%/\sqrt{E/\text{GeV}} \oplus 1\%$  and hadronic shower energies with  $\sigma(E)/E = 50\%/\sqrt{E/\text{GeV}} \oplus 2\%$ , as determined in test beam measurements [20]. In the backward region ( $153^\circ < \theta < 178^\circ$ ), the LAr calorimeter is complemented<sup>2</sup> by a lead–scintillating fibre spaghetti calorimeter (SpaCal) [21]. The LAr and SpaCal calorimeters are enclosed within the superconducting coil and are surrounded by an iron return yoke which is instrumented with streamer tubes to allow for the detection of muons in the range  $4^\circ < \theta < 171^\circ$ .

Dissociated proton states may be measured at small polar angles by a set of detectors in the forward direction: the PLUG, a sandwich calorimeter constructed from copper plates and silicon counters ( $0.6^\circ < \theta < 3.5^\circ$ ), the proton remnant tagger (PRT), an array of scintillators ( $0.06^\circ < \theta < 0.17^\circ$ ), and the drift chambers of the forward muon detector (FMD) [23] ( $3^\circ < \theta < 17^\circ$ ).

The luminosity is determined from the rate of Bethe-Heitler events  $ep \rightarrow e\gamma p$ , where the photon is detected in a calorimeter located downstream of the interaction point.

The events selected in this analysis are triggered by detecting electromagnetic clusters in the LAr or SpaCal calorimeter (electron trigger), by measuring a large missing transverse momentum in the LAr calorimeter ( $P_T^{\text{miss}}$  trigger), or by using hits in the muon detectors combined with central tracker signals (muon trigger). In the kinematic range of this analysis, events containing a pair of tau leptons are triggered with an efficiency of about 55% (35%) if one tau lepton decays leptonically (both tau leptons decay hadronically). Events containing single tau leptons and missing transverse momentum above 12 GeV (25 GeV) are triggered with an efficiency of about 50% (85%).

## 4 Particle Identification

### 4.1 Identification of electrons

An electron candidate is defined by the presence of a compact and isolated electromagnetic cluster of energy deposits in the LAr or SpaCal calorimeter. The kinematics of the electron candidate are measured from the calorimeter cluster. Among the charged tracks reconstructed in the event, the track with the lowest extrapolated distance of closest approach to the cluster ( $\delta$ ) is associated to the electron if it satisfies the condition  $\delta < 12$  cm. In this case, the azimuthal angle  $\phi$  and the charge of the electron are measured from the associated track. Additional energy within a cone of radius 0.5 in the pseudorapidity–azimuth ( $\eta$ – $\phi$ ) plane around the electron

<sup>2</sup>In 1994, a lead-scintillator calorimeter [22] was used instead.



candidate is required to be less than 3% of the energy attributed to the electron candidate. The electron identification efficiency is estimated using NC DIS events and is greater than 95% for an electron energy above 5 GeV.

## 4.2 Identification of muons

A muon candidate is identified by a track in the inner tracking system associated with a track segment or an energy deposit in the instrumented iron. The muon momentum is measured from the track curvature in the solenoidal magnetic field. The rejection of hadrons traversing the calorimeter and reaching the muon detectors is improved by requiring that the muon candidate deposits less than 5 GeV around its extrapolated track in the LAr calorimeter within a cylinder of radius 35 cm in the electromagnetic and 75 cm in the hadronic section. The efficiency to identify muons is estimated using elastic  $\gamma\gamma \rightarrow \mu^+\mu^-$  events and is greater than 85% in the energy range considered in this analysis.

## 4.3 Reconstruction of the hadronic final state

The hadronic final state (HFS) is measured [24] by combining energy measurements from the calorimeter with charged particle momenta measured by the inner tracker. Identified isolated electrons or muons are excluded from the HFS. The hadronic energy scale is calibrated by comparing the transverse momentum of well measured electrons to that of the HFS in NC DIS events [25]. Jets with  $P_T > 2$  GeV are reconstructed from HFS particles using an inclusive  $k_T$  algorithm [26] in the  $P_T$  recombination scheme with a separation parameter set to one.

## 4.4 Identification of tau decays

Leptonic tau decays (branching ratio 35% [27]) are identified by detecting an electron or a muon as described above. Hadronic tau decays typically produce low multiplicity, collimated, hadronic jets, henceforth denoted as  $\tau$ -jets. Depending on the number of charged hadrons produced, the hadronic decay modes are summed up in two categories, referred to as “1-prong” (one charged hadron, branching ratio 49%) and “3-prong” (three charged hadrons, branching ratio 14%). The branching ratio for decays into more than three charged hadrons is small (about 2%) and such decays are not considered in the present analysis.

Two different algorithms to identify hadronic tau decays, applied to jets reconstructed in the angular range  $20^\circ < \theta < 120^\circ$ , have been developed and are described below. The measurement of tau lepton pair production, in which the tau leptons generally have low momentum, requires an optimal background rejection. In contrast, the search for tau leptons produced in  $W$  decays at high  $P_T$  uses an algorithm that maximises the identification efficiency, since the signal cross section is low and the background is less severe.

## A: Neural Network based identification algorithm optimised for low $P_T$ taus

For the measurement of the tau lepton pair production, an algorithm has been developed that uses multiple neural networks to discriminate between  $\tau$ -jets and the background from electrons, muons or hadronic jets. A detailed description of the algorithm can be found in [28]. The algorithm is implemented in two steps.

In the first step, 1-prong (3-prong) candidates for hadronic tau decays are preselected by requiring exactly one (three) well reconstructed track(s) in the drift chambers within a cone (“ $\tau$ -cone”) around the jet axis. The opening angle of the  $\tau$ -cone varies between  $5^\circ$  and  $30^\circ$  depending on the jet momentum, with smaller angles at higher momentum due to the larger Lorentz boost in the direction of the tau candidate. The tracks are required to be not associated to identified electrons and muons and the scalar sum of their transverse momenta is required to be larger than 2 GeV. The fine granularity of the LAr calorimeter is used to match extrapolated tracks with energy deposits in the calorimeter and to reconstruct additional neutral particles associated to the tau candidate from unmatched energy deposits in the  $\tau$ -cone. The sum of the four-vectors of the tracks and of the neutral particles defines the  $\tau$ -jet four-vector. If all associated tracks have a well measured charge, the charge of the tau candidate is reconstructed as the sum of the charges of the associated tracks.

In the second step of the algorithm, various variables related to the particle multiplicity and collimation of the  $\tau$ -jet candidate are used. The set of variables includes: the multiplicity of the neutral clusters within the  $\tau$ -cone; the invariant masses calculated from clusters, from tracks and from charged and neutral particles in the  $\tau$ -cone; the difference in energy measured from tracks and from clusters; the distance in  $\eta - \phi$  between tracks and clusters; the first and second transverse moments of the distribution of energy deposits in the calorimeter with respect to the jet axis; the sum of energy deposits detected in an extended cone of radius 1.0 in  $\eta - \phi$  around the  $\tau$ -cone. Two neural networks (NN) using these variables are separately trained using MC simulations to identify 1-prong and 3-prong tau decay modes, the output of which is denoted by  $L^{1\text{-prong}}$  and  $L^{3\text{-prong}}$ , respectively. Their numerical value varies between zero and one and is used to discriminate between tau candidates (close to one) and hadronic jets (close to zero). Depending on the track multiplicity of the jet, the output of one of these NNs is used to select tau candidates. By requiring  $L^{1\text{-prong}} > 0.75$  (for 1-prong candidates) or  $L^{3\text{-prong}} > 0.75$  (for 3-prong candidates), the efficiency of this algorithm to identify hadronic tau lepton decays in  $\tau^+\tau^-$  events is about 50%, as calculated from MC simulations of tau decays with visible energy in the range considered in this analysis. The probability for hadronic jets to be misidentified as hadronic 1-prong (3-prong) tau decays is 0.5% (4%).

The signature of hadronic 1-prong tau decays may also be faked by unidentified electrons and muons. Two additional neural networks are trained to veto such cases. The output of these NNs, denoted by  $L_{\text{veto}}^e$  and  $L_{\text{veto}}^\mu$  respectively, is expected to be close to one for tau decays and close to zero for electrons or muons that fail the identification criteria described in sections 4.1 and 4.2.

## B: Identification algorithm optimised for high $P_T$ taus

A different approach to tau identification is used to search for events with a high momentum tau lepton and large  $P_T^{\text{miss}}$ . A high identification efficiency and a sufficient level of background

rejection are achieved by requiring a collimated jet, containing only one charged particle and isolated with respect to other tracks and jets within a cone of radius 1.0 in  $\eta$ - $\phi$ . The identification of hadronic  $\tau$ -decays is therefore restricted to hadronic 1-prong decay modes.

The collimation of a jet is measured by the jet radius  $R_{jet}$ , defined as the energy weighted average distance in  $\eta$ - $\phi$  between the jet axis and all HFS particles  $h$  (neutral and charged) in the jet:

$$R_{jet} = \frac{1}{E_{jet}} \sum_h E_h \sqrt{\Delta\eta(jet, h)^2 + \Delta\phi(jet, h)^2}. \quad (1)$$

Jets with one track and  $R_{jet} < 0.12$  are selected as tau candidates. The four-vector of the tau candidate is taken to be that of the jet. For jets with  $P_T > 7$  GeV, this identification procedure results in an efficiency of about 80% to identify 1-prong hadronic decays of tau leptons resulting from decays of  $W$  bosons. The misidentification probability for hadronic jets is less than 1%.

## 5 Production of $\tau^+\tau^-$ Pairs

### 5.1 Event selection

The decay modes investigated in the present analysis are classified as *leptonic* when both taus decay leptonically (branching ratio 6.2%, excluding decays to same flavour leptons), *semi-leptonic* when one tau decays hadronically and the second leptonically (45%) and *hadronic* when both taus decay hadronically (42%). The case where both tau leptons decay to charged leptons of the same flavour ( $ee$  or  $\mu\mu$  final state) is not included in the present analysis, as the separation of the  $\tau^+\tau^-$  signal from electron or muon pair production is difficult.

Leptonic and hadronic tau decays are identified as described in the previous section and by applying in addition the following selection criteria. The isolation of electrons and muons is measured by the distance in the  $\eta - \phi$  plane to the closest hadronic jet ( $D_{jet}$ ) and to the closest track ( $D_{track}$ ).

- $e$  candidates are reconstructed in the polar angular region  $20^\circ < \theta_e < 140^\circ$  and are required to have an energy above 5 GeV and a transverse momentum above 3 GeV. They must be isolated from jets with  $D_{jet} > 1.0$ .
- $\mu$  candidates are reconstructed in the polar angular region  $20^\circ < \theta_\mu < 140^\circ$  and are required to have a transverse momentum above 2 GeV. They must be isolated from other tracks and jets with  $D_{track} > 0.5$  and  $D_{jet} > 1.0$ , respectively.
- $\tau$ -jet candidates of transverse momenta above 2 GeV are reconstructed in the polar angular region  $20^\circ < \theta_\tau < 120^\circ$ , using algorithm **A** as described in section 4.4. The output of the neural network is required to satisfy  $L^{1\text{-prong}} > 0.75$  or  $L^{3\text{-prong}} > 0.75$ .

Events with two tau candidates are selected. If the charge of both tau candidates is measured, events with two candidates of the same charge are rejected.

In order to avoid significant background contributions from NC DIS and  $\gamma p$  processes, the analysis is restricted to elastic  $ep \rightarrow ep\tau^+\tau^-$  production. Inelastic events are vetoed by requiring no extra track or energy deposit above the noise level in the main detector in addition to those associated to the decay products of both tau leptons and a possible additional electron. Furthermore, no significant activity should be observed in the forward detectors (PLUG, FMD and PRT). The requirements applied [29] ensure that the proton remains intact or dissociates into a low mass state. Remaining background originates mainly from elastic lepton pair production and from diffractive NC DIS or  $\gamma p$  processes.

Electron and muon pair production processes ( $\gamma\gamma \rightarrow e^+e^-$  and  $\gamma\gamma \rightarrow \mu^+\mu^-$ ) constitute a background to tau pair production in semi-leptonic decay modes when one of the leptons is correctly identified as  $e$  or  $\mu$  while the second lepton fails to be identified by the algorithms described in sections 4.1 and 4.2 and fakes the signature of a 1-prong hadronic tau decay. In order to reject this background,  $L_{\text{veto}}^e > 0.75$  ( $L_{\text{veto}}^\mu > 0.75$ ) is required for 1-prong tau jet candidates selected in the  $e + \tau$ -jet ( $\mu + \tau$ -jet) channel.

To further reduce the background from NC DIS processes, where the scattered electron is selected as a candidate for a  $\tau \rightarrow e$  decay and the struck quark fragments into a collimated jet of low particle multiplicity that fakes the  $\tau$ -jet signature, the longitudinal momentum balance calculated as

$$E - P_z = \sum_i E_i(1 - \cos \theta_i) \quad (2)$$

is employed, where  $E_i$  and  $\theta_i$  denote the energy and polar angle of each particle detected in the event. For events in which only momentum in the proton direction is undetected,  $E - P_z$  is equal to twice the energy  $E_e$  of the electron beam, i.e. 55.2 GeV. For events containing tau leptons,  $E - P_z$  values well below 55.2 GeV are expected since the neutrinos produced in the tau decays are not detected and, most of the time, the scattered beam electron escapes down the beam pipe. By requiring  $E - P_z < 50$  GeV when the detected electron has the same charge as the beam lepton, the NC DIS background is rejected to a large extent. The  $E - P_z$  cut is also applied to the leptonic channel and rejects muon pair-production events, for which the scattered electron is detected together with one produced muon while the second muon escapes in the forward direction. If a second electron is detected in the event, this condition is not applied.

The selection criteria for  $\tau^+\tau^-$  events are summarised in table 1. With these selection criteria, 1.2% of the elastic  $\gamma\gamma \rightarrow \tau^+\tau^-$  events in which both tau leptons satisfy  $P_T^\tau > 2$  GeV and  $20^\circ < \theta_\tau < 140^\circ$  are selected. The efficiency is limited by the fact that the energy of the detected tau decay products is significantly lower than the tau lepton energy, since the neutrinos escape detection.

## 5.2 Background studies

Due to the aforementioned elasticity requirements, the remaining background from NC DIS and  $\gamma p$  processes consists mainly of exclusive diffractive events, for which the validity of the resolved pomeron model [30] as implemented in the RAPGAP program is questionable. Hence

Selection of $\tau^+\tau^-$ Events				
Decay Channel	Leptonic	Semi-leptonic		Hadronic
$\tau$ Signatures	$e$	$e$	$\mu$	$\tau$ -jet
	$\mu$	$\tau$ -jet	$\tau$ -jet	$\tau$ -jet
	Events with two same charge tau candidates rejected			
Elastic Production	No additional tracks, no additional clusters in the LAr or SpaCal calorimeter, no activity in forward detectors above noise level			
Background Reduction		$L_{\text{veto}}^e > 0.75^{(1)}$	$L_{\text{veto}}^\mu > 0.75^{(1)}$	
	$E - P_z < 50 \text{ GeV}^{(2)}$			
<p><sup>(1)</sup> applied only to 1-prong <math>\tau</math>-jet candidates</p> <p><sup>(2)</sup> applied only if the electron associated with the tau decay has the same charge as the beam lepton and no second electron is detected</p>				

Table 1: Selection criteria for elastic  $\tau^+\tau^-$  events in the leptonic ( $e + \mu$ ), semi-leptonic ( $e + \tau$ -jet,  $\mu + \tau$ -jet) and hadronic ( $\tau$ -jet +  $\tau$ -jet) decay modes of the  $\tau$  lepton pair.

the RAPGAP prediction for NC DIS ( $\gamma p$ ) is normalised to the number of events observed in a control sample in which an electron and a jet (two jets) are selected in the  $P_T$  and  $\theta$  ranges of the analysis, and where the elastic requirements are applied. It has been verified that the shapes of the observed kinematic distributions are reasonably well described by RAPGAP.

Furthermore, to check that the probability for an electron, a muon or a hadronic jet to be misidentified as a  $\tau$ -jet candidate is well described by the MC simulation, several event samples are studied in which the contribution of individual background processes is enhanced. These event samples are selected in a phase space similar to that of the  $\tau^+\tau^-$  event sample, requiring the conditions for elastic production to be fulfilled. In order to enhance the background component in the control samples, the condition  $L^{1\text{-prong}} > 0.75$  or  $L^{3\text{-prong}} > 0.75$  on the NN outputs for  $\tau$ -jet candidates is not applied.

The following samples are employed:

- **$\gamma\gamma \rightarrow e^+e^-$  control sample**

A  $\gamma\gamma \rightarrow e^+e^-$  dominated event sample is defined by selecting events with one electron and one 1-prong  $\tau$ -jet candidate. No veto condition on  $L_{\text{veto}}^e$  is applied. Events with two same charge tau candidates are rejected.

- **$\gamma\gamma \rightarrow \mu^+\mu^-$  control sample**

A  $\gamma\gamma \rightarrow \mu^+\mu^-$  enriched event sample is defined by selecting events with one muon and one 1-prong  $\tau$ -jet candidate. No veto condition on  $L_{\text{veto}}^\mu$  is applied. Events with two same charge tau candidates are rejected.

- **$\gamma p$  control sample**

A  $\gamma p$  enriched event sample is defined by selecting events containing two jets with one, two or three tracks. If both jets are 1-prong tau candidates, the requirements  $L_{veto}^e > 0.75$  and  $L_{veto}^\mu > 0.75$  are applied to suppress the contributions from  $\gamma\gamma \rightarrow e^+e^-$  and  $\gamma\gamma \rightarrow \mu^+\mu^-$  processes. In order to reduce the contribution from NC DIS process, only events with  $E - P_z < 45$  GeV are accepted.

- **NC DIS control sample**

A NC DIS enriched event sample is defined by selecting events with one electron and one  $\tau$ -jet candidate. If the  $\tau$ -jet is a 1-prong candidate,  $L_{veto}^e > 0.75$  is required in order to suppress the contribution from  $\gamma\gamma \rightarrow e^+e^-$  processes.

The selection criteria of the background control samples are summarised in table 2, in which the numbers of events obtained from the data and the MC simulation are also given.

The distributions of all quantities used in the selection of the  $\tau^+\tau^-$  event sample are well described by the MC simulation both in shape and normalisation in the control samples. Examples of these distributions are shown in figure 2. The distributions of the electron and muon rejection discriminators  $L_{veto}^e$  and  $L_{veto}^\mu$  are shown in figures 2a and 2b for the control samples where most of the tau candidates are unidentified electrons and muons, respectively. The distribution of the NN output  $L^{1\text{-prong}}$  ( $L^{3\text{-prong}}$ ) is shown in figure 2c (2d) for 1-prong (3-prong) jets in the  $\gamma p$  control sample which is enriched in hadronic jets. In figures 2a–d the contribution from tau pair production populates the region close to one, while the background accumulates at values close to zero, as expected. Finally, the distribution of the  $E - P_z$  variable is shown in figure 2e for the NC DIS control sample. The agreement between data and simulation in the control samples shows that the background contribution as well as the experimental efficiencies are modelled by the MC simulation within the attributed systematic uncertainties described in the next section.

### 5.3 Systematic uncertainties

In this section, the systematic uncertainties associated with the measurement of elastic  $\tau^+\tau^-$  production are discussed. The uncertainties on the signal expectation are determined by varying the following experimental quantities by  $\pm 1$  standard deviation.

- **Electron identification and reconstruction**

In the kinematic region considered in the  $\tau^+\tau^-$  analysis, the uncertainty on the electron identification efficiency is 5% (2% when the electron energy is above 10 GeV). The electron energy scale uncertainty is estimated to be 3%. The uncertainties on the measurement of the electron angles  $\theta$  and  $\phi$  are 3 mrad and 1 mrad, respectively.

- **Muon identification and reconstruction**

The uncertainty on the muon identification efficiency is 5%. The relative scale uncertainty on the muon momentum is conservatively taken to be 5%. The uncertainties on the measurements of the muon angles  $\theta$  and  $\phi$  are 3 mrad and 1 mrad, respectively.

$\tau^+\tau^-$ Background Control Samples				
Control samples	$e^+e^-$	$\mu^+\mu^-$	$\gamma p$	NC DIS
Signatures	$e$ 1-prong $\tau$ -jet	$\mu$ 1-prong $\tau$ -jet	two jets with $\leq 3$ tracks	$e$ $\tau$ -jet
	Events with two same charge tau candidates rejected			
Elastic Production	No additional tracks, no additional clusters in the LAr or SpaCal calorimeter, no activity in forward detectors above noise level			
Background Reduction			$L_{\text{veto}}^e > 0.75^{(1)}$ $L_{\text{veto}}^\mu > 0.75^{(1)}$ $E - P_z < 45$ GeV	$L_{\text{veto}}^e > 0.75^{(2)}$
H1 Data	115	20	29	29
Total SM	$133.1 \pm 19.5$ (95% $e^+e^-$ )	$14.1 \pm 1.4$ (50% $\mu^+\mu^-$ )	$24.9 \pm 10.0$ (79% $\gamma p$ )	$32.4 \pm 6.3$ (62% NC DIS)
(1) applied only if both jets are 1-prong tau candidates				
(2) applied only to 1-prong $\tau$ -jet candidates				

Table 2: Selection criteria for the background control samples in which each background contribution is individually enhanced. The numbers of observed and expected events are also shown. The dominant contribution to the total SM expectation is indicated as a percentage in the last row. Here, the tau candidates are not required to satisfy the condition  $L^{1\text{-prong}} > 0.75$  or  $L^{3\text{-prong}} > 0.75$ .

- **Identification and reconstruction of hadronic tau decays**

For each of the charged tracks associated to the  $\tau$ -jet, a reconstruction efficiency uncertainty of 3% is assigned. The efficiency to identify hadronic  $\tau$  decays with the NN algorithm **A** has an additional uncertainty of 10% [28], estimated by comparing different simulations of shower development in the LAr calorimeter. It has been verified, using a large statistics sample of hadronic jets from inclusive CC DIS and NC DIS samples, that the output of both NNs is well described by the MC simulation. The uncertainties arising from the modelling of tau decays are negligible, as estimated by comparing the results obtained using either the PYTHIA [31] or TAUOLA [32] programs to simulate the decays of the tau leptons generated with GRAPE. The energy of the neutral clusters of  $\tau$ -jet candidates has a relative uncertainty of 4%, corresponding to the hadronic energy scale uncertainty. The uncertainties on the measurements of the  $\tau$ -jet angles  $\theta$  and  $\phi$  are

estimated to be 10 mrad and 5 mrad, respectively.

- **Elastic event selection**

The efficiency with which elastic events are selected and proton dissociative events are rejected depends on the noise level in the LAr and on the performance of the forward detectors [29]. Its uncertainty does not exceed 3%.

- **Triggering**

The trigger efficiency is studied using elastic  $e^+e^-$  and  $\mu^+\mu^-$  events and diffractive  $\gamma p$  di-jet events in a phase space similar to that of the  $\tau^+\tau^-$  analysis. The uncertainty on the trigger efficiency depends on the region in  $\theta$  in which the tau candidates are detected: central ( $\theta > 30^\circ$ ) or forward ( $\theta < 30^\circ$ ). The uncertainty is 10% if both tau candidates are in the central region, 20% if one tau candidate is detected in the forward and the other in the central region and 30% if both tau candidates are detected in the forward region.

- **Luminosity**

The luminosity of the analysed datasets is measured with an uncertainty of 1.5%.

The individual effects of the above experimental uncertainties are combined in quadrature, yielding a total uncertainty of 21% on the signal expectation. The largest contributions to this uncertainty arise from systematics attributed to the tau identification procedure (15%) and to the trigger efficiency (12%).

Contributions from background processes, modelled using the generators described in section 2, are attributed relative systematic uncertainties of 50% ( $\gamma p$ ), 30% (NC DIS), 15% ( $\gamma\gamma \rightarrow e^+e^-$ ,  $\gamma\gamma \rightarrow \mu^+\mu^-$ ), estimated from the level of agreement observed between the MC simulation and the data in the background enhanced control samples described in section 5.2.

## 5.4 Results

In total, 30  $\tau^+\tau^-$  candidate events are selected, in agreement with the SM expectation of  $27.1 \pm 4.1$  events, of which  $16.0 \pm 3.4$  are expected from  $\gamma\gamma \rightarrow \tau^+\tau^-$  signal processes. The signal expectation is dominated (85%) by the elastic production component. The lepton pair production, NC DIS and  $\gamma p$  processes contribute with similar rates to the background expectation. The numbers of observed and expected events in the four analysed channels are shown in table 3. An event selected in the semi-leptonic channel is displayed in figure 3.

The distributions of the polar angle and of the transverse momentum of the tau candidates, together with the visible invariant mass, are shown in figure 4. The measured distributions are compatible with the SM expectations. As expected for  $\gamma\gamma \rightarrow \tau^+\tau^-$  processes, most tau decay products are detected with relatively small transverse momenta.

Using the selected sample, a measurement of the cross section for the elastic production of  $\tau^+\tau^-$  pairs is performed in the kinematic region defined by  $20^\circ < \theta_\tau < 140^\circ$  and  $P_T^\tau > 2$  GeV. For this measurement, the data samples collected at  $\sqrt{s} = 301$  GeV and 319 GeV are combined, taking into account their respective luminosities. Assuming a linear dependence of



$\tau^+\tau^-$ Results					
Decay Channel	Leptonic $e\mu$	Semi-leptonic		Hadronic $\tau\text{-jet}\tau\text{-jet}$	Total
		$e\tau\text{-jet}$	$\mu\tau\text{-jet}$		
H1 Data	7	2	10	11	30
SM	$2.9 \pm 0.4$	$6.3 \pm 0.9$	$7.0 \pm 1.3$	$11.0 \pm 2.0$	$27.1 \pm 4.1$
$\tau^+\tau^-$	56%	47%	85%	50%	59%

Table 3: Number of selected events and SM prediction for the  $\tau^+\tau^-$  analysis. The expected relative contribution of the  $\tau^+\tau^-$  process to the SM prediction is also shown.

the cross section on the proton beam energy, as predicted by the SM, the measured cross section corresponds to an effective centre-of-mass energy of  $\sqrt{s} = 314$  GeV. The cross section is calculated using the formula:

$$\sigma = \frac{N_{\text{data}} - N_{\text{bgr}}}{\mathcal{L} \cdot A}, \quad (3)$$

where  $N_{\text{data}}$  is the number of observed events,  $N_{\text{bgr}}$  the expected contribution from background processes,  $\mathcal{L}$  the total integrated luminosity and  $A$  the signal acceptance. The contribution from inelastic  $\gamma\gamma \rightarrow \tau^+\tau^-$  processes is included in the background expectation. The signal acceptance  $A$  is calculated using the GRAPE generator, as the ratio of the number of events accepted at reconstructed level to the number of events generated in the defined phase space. It accounts for the selection and trigger efficiencies and for the differences in momentum between the original  $\tau$  leptons and the detected decay products.

The measured cross section for elastic tau pair production  $ep \rightarrow ep\tau^+\tau^-$  integrated over the phase space defined above is  $13.6 \pm 4.4 \pm 3.7$  pb where the first error is statistical and the second systematic. The result is in agreement with the SM expectation of  $11.2 \pm 0.3$  pb, calculated using the GRAPE generator.

## 6 Production of High $P_T$ Tau Leptons in Events with Large Missing Transverse Momentum

### 6.1 Event selection

Events containing an isolated tau lepton and large missing transverse momentum are selected with a procedure similar to that used in the analysis of events with an isolated electron or muon and large missing transverse momentum [7]. The tau leptons are identified using hadronic decays only, as the leptonic tau decays lead to final states which cannot be distinguished from those studied in [7].

The event selection is performed in two steps. In the first step, the net transverse momentum reconstructed from all particles (electrons, muons and hadrons)  $P_T^{\text{miss}}$ , is required to be above 12 GeV. In order to ensure uniform trigger conditions, the net transverse momentum measured

from all energy deposits detected in the calorimeter,  $P_T^{\text{calo}}$ , is required to be above 12 GeV. The reconstructed  $P_T^{\text{miss}}$  is approximately equal to  $P_T^{\text{calo}}$  except for events containing muons in the final state. In order to exploit further the event topology in the transverse plane, the variable  $V_{ap}/V_p$  is employed, defined as the ratio of the anti-parallel to parallel projections of all energy deposits in the calorimeter with respect to the direction of  $P_T^{\text{calo}}$  [33]. Events with genuine missing transverse momentum are in general reconstructed with  $V_{ap}/V_p$  values close to zero and large values of  $P_T^{\text{calo}}$ , whereas background events from NC DIS and  $\gamma p$  processes are intrinsically balanced, with larger values of  $V_{ap}/V_p$  and low values of  $P_T^{\text{calo}}$ . Only events with  $V_{ap}/V_p$  below 0.5 are accepted. For events with  $P_T^{\text{calo}}$  below 25 GeV, a stricter condition of  $V_{ap}/V_p < 0.15$  is applied. The background from NC DIS is further reduced by requiring  $E - P_z < 50$  GeV. Additionally, the events are required to contain at least one isolated hadronic jet with transverse momentum above 7 GeV in the central region of the detector  $20^\circ < \theta_{jet} < 120^\circ$ . The isolation is characterised by the distance of the jet in  $\eta - \phi$  to the nearest hadronic jet ( $D_{jet} > 1.0$ ) and the nearest track not belonging to the jet ( $D_{track} > 1.0$ ).

In the second selection step, the isolated jets are required to pass the tau identification criteria of algorithm **B** described in section 4.4. A jet is accepted if it is narrow ( $R_{jet} < 0.12$ ) and contains exactly one charged track ( $N_{tracks}^{jet} = 1$ ). In order to remove background from hadronic jets containing mostly neutral particles, this track is required to have a transverse momentum  $P_T^{track}$  greater than 5 GeV. If more than one isolated jet satisfies these requirements, the one with the highest  $P_T$  is considered as the tau candidate. In order to further reduce the background from intrinsically balanced events, in which the  $P_T^{\text{miss}}$  is due to a mismeasurement, the acoplanarity  $\Delta\phi$ , defined as the angle in the transverse plane between the  $\tau$ -jet candidate and the hadronic system excluding the tau candidate ( $X$ ), is required to be below  $170^\circ$ . This criterium removes events in which the  $\tau$ -jet candidate and the rest of the hadronic system are back-to-back, as is typical for NC DIS and  $\gamma p$  events.

A summary of all selection criteria is presented in table 4. Using these selection criteria, SM  $W \rightarrow \tau\nu$  events are selected with an overall efficiency of 8%. In comparison to  $W$  decays into electrons or muons [7],  $W \rightarrow \tau\nu$  decays are selected with a significantly lower efficiency, mainly due to the branching ratio (49%) for hadronic 1-prong tau decays and to the more restricted polar angular range of this analysis.

## 6.2 Background studies

After applying the selection criteria, the main background is expected to occur from events with genuine missing transverse momentum produced by CC DIS processes, in which a narrow jet with low track multiplicity fakes the tau signature. Additional background arises from NC DIS and  $\gamma p$  processes, which have a much larger cross section than the CC DIS process and lead to events that contain hadronic jets but no genuine  $P_T^{\text{miss}}$ . The modelling of the CC DIS, NC DIS and  $\gamma p$  backgrounds is verified using samples in which the contribution of each background process is enhanced. The selection criteria defining the background control samples are listed in table 5, together with the observed number of events and the SM expectation.

The CC DIS background control sample is selected using the “ $P_T^{\text{miss}}$  + isolated jet” preselection described in section 6.1. The NC DIS and  $\gamma p$  samples are selected in a complementary

<b>Selection of <math>\tau + P_T^{\text{miss}}</math> Events</b>	
<b><math>P_T^{\text{miss}}</math> + Isolated Jet Preselection</b>	$P_T^{\text{calo}} > 12 \text{ GeV}$
	$P_T^{\text{miss}} > 12 \text{ GeV}$
	$E - P_z < 50 \text{ GeV}$
	$V_{ap}/V_p < 0.5$ ( $< 0.15$ for $P_T^{\text{calo}} < 25 \text{ GeV}$ )
	$N_{jets} > 1$
	$P_T^{\text{jet}} > 7 \text{ GeV}$
	$20^\circ < \theta_{jet} < 120^\circ$
	$D_{track} > 1.0$
<b>Final <math>\tau + P_T^{\text{miss}}</math> Selection</b>	$N_{tracks}^{\text{jet}} = 1$
	$P_T^{\text{track}} > 5 \text{ GeV}$
	$R_{jet} < 0.12$
	$\Delta\phi < 170^\circ$

Table 4: Selection criteria for events containing an isolated  $\tau$  lepton and large  $P_T^{\text{miss}}$ .

phase space at large  $E - P_z$  and large  $V_{ap}/V_p$ , respectively. In these background samples the tight selection criteria of tau candidates are not applied and only isolated jets, as defined in table 4, are considered.

As shown in figure 5a–c, the distributions of  $R_{jet}$ ,  $N_{tracks}^{\text{jet}}$ , and  $P_T^{\text{track}}$  in the CC DIS control sample are well described by the MC simulation, both in shape and normalisation. The distribution of the acoplanarity angle  $\Delta\phi$  in the control sample enriched in  $\gamma p$  events, shown in figure 5d, shows a clear peak towards  $180^\circ$ , corresponding to back-to-back events. In figure 5e the distribution of the hadronic transverse momentum  $P_T^X$  for the NC DIS control sample is shown. The good agreement between data and MC simulation observed in all control samples confirms the good understanding of background rates and of the properties of the jets (shape and multiplicity) used in the tau identification procedure.

### 6.3 Systematic uncertainties

In this section, the systematic uncertainties associated with the search for events containing an isolated tau lepton and large missing transverse momentum are discussed. The effect of those uncertainties on the expectations from SM W production and from background processes is determined by varying the experimental quantities by  $\pm 1$  standard deviation.

$\tau + P_T^{\text{miss}}$ Background Control Samples			
Control Sample	CC DIS	NC DIS	$\gamma P$
Selection	$P_T^{\text{miss}} > 12 \text{ GeV}, P_T^{\text{calo}} > 12 \text{ GeV},$ at least one isolated jet		
	$E - P_z < 50 \text{ GeV}$	$E - P_z > 35 \text{ GeV}$	$E - P_z < 50 \text{ GeV}$
	$V_{ap}/V_p < 0.5$	$P_T^e > 10 \text{ GeV}$	$V_{ap}/V_p > 0.15$
	$V_{ap}/V_p < 0.15$ for $P_T^{\text{calo}} < 25 \text{ GeV}$	$5^\circ < \theta^e < 150^\circ$	no electrons
Data	1811	108	1165
Total SM	$1858.6 \pm 120.7$	$100.3 \pm 22.0$	$1173.1 \pm 208.3$
	(93% CC)	(98% NC)	(80% $\gamma P$ )

Table 5: Selection criteria for the  $\tau + P_T^{\text{miss}}$  background control samples together with the number of selected events compared to the SM expectation. The dominant contribution to the SM prediction is indicated as a percentage in the last row of the table.

- **Tau identification procedure**

The main experimental uncertainty on the signal and background expectations arises from the requirement of exactly one track within the jet and from the condition on the jet radius  $R_{jet} < 0.12$ . The energy of charged tracks is reconstructed with an uncertainty of 5%. The measurements of the polar and azimuthal angles are attributed a systematic error of 3 mrad and 1 mrad respectively. The uncertainty on the track reconstruction efficiency is 3% and has a relatively large effect on the background expectation, due to migrations of hadronic jets with multiple charged particles into the single track category. The modelling of  $R_{jet}$  is studied with high statistical precision using jets in a dedicated inclusive NC DIS sample. The measured and simulated jet radius distributions are compared and an uncertainty depending on the polar angle of the  $\tau$ -jet is attributed to  $R_{jet}$ . The uncertainties associated with the tau identification are 15% for the expected  $W$  signal and 25% for the background predictions.

- **Hadronic final state reconstruction**

The hadronic energy measurement has a relative uncertainty of 4%. The polar angle measurement has an uncertainty varying from 3 mrad for jets reconstructed in the central region to 10 mrad for forward jets. The topological variable  $V_{ap}/V_p$  is attributed a relative uncertainty of 10%.

- **Trigger**

The uncertainty on the  $P_T^{\text{miss}}$  trigger efficiency is 5% deduced from a large statistics NC DIS sample for which the trigger information is reconstructed offline, ignoring the signal from the electron [33].

- **Luminosity**

The luminosity of the analysed datasets is measured with an uncertainty of 1.5%.

- **Theoretical errors on signal and background contributions**

The uncertainty on the  $W$  production signal cross section is estimated to be 15% [12]. The expectations from NC DIS and  $\gamma p$  processes are each attributed an additional uncertainty of 20%, a value which has been estimated from the control samples described in section 6.2. This uncertainty covers the sensitivity of the jet radius and multiplicity (used in the tau identification algorithm) to the modelling of parton showers in NC DIS and  $\gamma p$  MC samples.

The individual effects of the experimental uncertainties are combined in quadrature to give the total experimental systematic uncertainty. The total uncertainty on the SM  $W$  signal is 20% and that on the SM background is 34%. For both signal and background processes, the total uncertainty is dominated by the uncertainty arising from the tau identification procedure and the theoretical uncertainties.

## 6.4 Results

In the final event sample 6 events are observed in the data, compared to a total SM expectation of  $9.9^{+2.5}_{-3.6}$  events, of which  $0.89^{+0.15}_{-0.26}$  are expected from SM  $W$  production. The  $P_T^X$  spectrum and other properties of the events in the final sample are shown in figure 6. Table 6 summarises the results. The events observed in the data are concentrated in the region of very low  $P_T^X$ , where the contribution from CC DIS background processes dominates the SM expectation. In the region  $P_T^X > 25$  GeV, where an excess of events containing isolated electrons or muons is observed [7], no event is found for a SM prediction of  $0.39 \pm 0.10$ , of which  $0.20 \pm 0.04$  are expected from SM  $W$  production.

In the absence of a signal, a model independent upper limit on the cross section for the production of events containing an isolated tau leptons and large missing transverse momentum is set in the kinematic region:  $5^\circ < \theta_\tau < 140^\circ$ ,  $P_T^\tau > 10$  GeV and  $P_T^{\text{miss}} > 12$  GeV. The limit is calculated using a modified frequentist approach based on likelihood ratios [34] and taking into account the systematic uncertainties discussed in section 6.3. The acceptance for processes producing isolated tau leptons in events with large missing transverse momentum in the given kinematic region is estimated using the MC simulation for SM  $W$  production, implemented in the EPVEC generator. An additional model uncertainty of 10% is attributed to the acceptance. This uncertainty is estimated by comparing the acceptance predicted by EPVEC with that obtained using the generator ANOTOP, which simulates the anomalous production of single top quarks in  $ep$  collisions at HERA [35] and produces  $W$  bosons with different kinematic distributions<sup>3</sup>.

An upper limit of  $\sigma < 0.85$  pb at 95% confidence level is obtained for the production cross section of events containing an isolated tau lepton and large missing transverse momentum in the phase space defined above. In the region  $P_T^X > 25$  GeV, the upper limit is

---

<sup>3</sup>The  $P_T^X$  distribution for top events is peaked at about 70 GeV, while events from SM  $W$  production are concentrated at low  $P_T^X$  values.

$\tau + P_T^{\text{miss}}$ Results	H1 Data	SM Expectation	SM Signal	Other SM Processes
Total	6	$9.9^{+2.5}_{-3.6}$	$0.89^{+0.15}_{-0.26}$	$9.0^{+2.5}_{-3.6}$
$P_T^X > 25 \text{ GeV}$	0	$0.39^{+0.09}_{-0.11}$	$0.20^{+0.04}_{-0.05}$	$0.19^{+0.08}_{-0.10}$
$P_T^X > 40 \text{ GeV}$	0	$0.16^{+0.07}_{-0.06}$	$0.08^{+0.02}_{-0.02}$	$0.08^{+0.07}_{-0.06}$

Table 6: Number of events observed in the data compared to the SM expectation for signal ( $W$  decay into  $\tau$ ) and background processes in the final  $\tau + P_T^{\text{miss}}$  sample.

$\sigma(P_T^X > 25 \text{ GeV}) < 0.31 \text{ pb}$  at 95% confidence level. These limits are higher than the cross sections measured in the electron and muon channels [7]. The present measurement is therefore compatible with the previous measurement of events with an electron or muon and  $P_T^{\text{miss}}$ , as expected if lepton universality is assumed.

## 7 Summary

In this paper, the production of tau leptons in  $ep$  collisions at HERA is investigated in events containing a  $\tau^+\tau^-$  pair and events containing an isolated tau lepton and large missing transverse momentum.

The production cross section of  $\tau^+\tau^-$  pairs is measured in elastic processes, in a combination of leptonic, semi-leptonic and hadronic decay modes of the two tau leptons. In a data sample corresponding to an integrated luminosity of  $106 \text{ pb}^{-1}$ , 30 events are observed, in agreement with a Standard Model expectation of  $27.1 \pm 4.1$  events, of which  $16.0 \pm 3.4$  are expected from  $\gamma\gamma \rightarrow \tau^+\tau^-$  signal processes. This is the first observation of tau pair production in  $ep$  collisions.

A search for the production of isolated tau leptons in events with large missing transverse momentum is performed in a data sample corresponding to an integrated luminosity of  $115 \text{ pb}^{-1}$ . The selection yields 6 candidate events, compatible with a Standard Model expectation of  $9.9^{+2.5}_{-3.6}$  events. No event is observed in the region  $P_T^X > 25 \text{ GeV}$ , where  $0.39 \pm 0.10$  events are expected, including  $0.20 \pm 0.05$  events from  $W \rightarrow \tau\nu_\tau$  decays. An upper limit on the production cross section of  $\sigma(P_T^X > 25 \text{ GeV}) < 0.31 \text{ pb}$  at 95% confidence level is set.

## Acknowledgements

We are grateful to the HERA machine group whose outstanding efforts have made this experiment possible. We thank the engineers and technicians for their work in constructing and maintaining the H1 detector, our funding agencies for financial support, the DESY technical staff for continual assistance and the DESY directorate for support and for the hospitality which they extend to the non-DESY members of the collaboration.

## References

- [1] J. A. M. Vermaseren, Nucl. Phys. B **229** (1983) 347.
- [2] U. Baur, J. A. M. Vermaseren and D. Zeppenfeld, Nucl. Phys. B **375** (1992) 3.
- [3] A. Aktas *et al.* [H1 Collaboration], Eur. Phys. J. C **31** (2003) 17 [hep-ex/0307015].
- [4] A. Aktas *et al.* [H1 Collaboration], Phys. Lett. B **583** (2004) 28 [hep-ex/0311015].
- [5] T. Ahmed *et al.* [H1 Collaboration], DESY 94-248 (1994).
- [6] C. Adloff *et al.* [H1 Collaboration], Eur. Phys. J. C **5** (1998) 575 [hep-ex/9806009].
- [7] V. Andreev *et al.* [H1 Collaboration], Phys. Lett. B **561** (2003) 241 [hep-ex/0301030].
- [8] J. Breitweg *et al.* [ZEUS Collaboration], Phys. Lett. B **471** (2000) 411 [hep-ex/9907023].
- [9] S. Chekanov *et al.* [ZEUS Collaboration], Phys. Lett. B **559** (2003) 153 [hep-ex/0302010].
- [10] S. Chekanov *et al.* [ZEUS Collaboration], Phys. Lett. B **583** (2004) 41 [hep-ex/0311028].
- [11] GRAPE 1.1, T. Abe, Comput. Phys. Commun. **136** (2001) 126 [hep-ph/0012029].
- [12] K.–P. Diener, C. Schwanenberger and M. Spira, Eur. Phys. J. C **25** (2002) 405 [hep-ph/0203269];  
P. Nason, R. Rückl and M. Spira, J. Phys. G **25** (1999) 1434 [hep-ph/9902296];  
M. Spira, Proc. of the Workshop “Monte Carlo Generators for HERA Physics” (1991),  
Eds. A. T. Doyle, G. Grindhammer, G. Ingelman, H. Jung, p. 623 [hep-ph/9905469].
- [13] K.–P. Diener, C. Schwanenberger and M. Spira, hep-ex/0302040.
- [14] H. Jung, Comput. Phys. Commun. **86** (1995) 147;  
RAPGAP program manual (1998) unpublished  
<http://www-h1.desy.de/~jung/RAPGAP.html>.
- [15] PYTHIA 5.7, T. Sjöstrand, Comput. Phys. Commun. **82** (1994) 74.
- [16] DJANGO 2.1, G.A. Schüller and H. Spiesberger, Proc. of the Workshop “Physics at HERA” (1991), Eds. W. Buchmüller and G. Ingelman, Vol. 3, p. 1419.
- [17] GEANT 3, R. Brun *et al.*, CERN-DD/EE/84-1.
- [18] I. Abt *et al.* [H1 Collaboration], Nucl. Instrum. Meth. A **386** (1997) 310 and 348.
- [19] B. Andrieu *et al.* [H1 Calorimeter Group], Nucl. Instrum. Meth. A **336** (1993) 460.
- [20] B. Andrieu *et al.* [H1 Calorimeter Group], Nucl. Instrum. Meth. A **336** (1993) 499;  
B. Andrieu *et al.* [H1 Calorimeter Group], Nucl. Instrum. Meth. A **344** (1994) 492;  
B. Andrieu *et al.* [H1 Calorimeter Group], Nucl. Instrum. Meth. A **350** (1994) 57.
- [21] R. D. Appuhn *et al.* [H1 SpaCal Group], Nucl. Instrum. Meth. A **386** (1997) 397.

- [22] J. Ban *et al.* [H1 BEMC Group], Nucl. Instrum. Meth. A **372** (1996) 399.
- [23] I. R. Kenyon *et al.* [H1 FMD group], Nucl. Instrum. Meth. A **340** (1994) 304.
- [24] M. Peez, “Recherche de déviations au-delà du Modèle Standard dans les processus de grande énergie transverse sur le collisionneur électron-proton HERA”, PhD Thesis, Aix-Marseille University, 2003,  
available at [http://www-h1.desy.de/publications/theses\\_list.html](http://www-h1.desy.de/publications/theses_list.html).
- [25] B. Portheault, “Première mesure des sections efficaces de courant chargé et neutre avec le faisceau de positrons polarisé à HERA II et analyses QCD-électrofaibles”, PhD Thesis, Paris-Sud XI University, 2005,  
available at [http://www-h1.desy.de/publications/theses\\_list.html](http://www-h1.desy.de/publications/theses_list.html).
- [26] S. D. Ellis and D. E. Soper, Phys. Rev. D **48** (1993) 3160 [hep-ph/9305266];  
S. Catani, Y. L. Dokshitzer, M. H. Seymour and B. R. Webber, Nucl. Phys. B **406** (1993) 187;  
C. Adloff *et al.* [H1 Collaboration], Nucl. Phys. B **545** (1999) 3 [hep-ex/9901010].
- [27] S. Eidelman *et al.* [Particle Data Group], Phys. Lett. B **592** (2004) 1.
- [28] C. Veelken, “Search for Events with Isolated Leptons and Large Missing Transverse Momentum in  $ep$  Collisions at HERA”, PhD Thesis, University of Liverpool, 2006,  
available at [http://www-h1.desy.de/publications/theses\\_list.html](http://www-h1.desy.de/publications/theses_list.html).
- [29] P. Laycock, “A Measurement of the Diffractive Reduced Cross-Section  $\sigma_r^D(3)$  at High  $Q^2$  with the H1 Detector at HERA”, PhD Thesis, University of Liverpool, 2003,  
available at [http://www-h1.desy.de/publications/theses\\_list.html](http://www-h1.desy.de/publications/theses_list.html).
- [30] G. Ingelman and P. E. Schlein, Phys. Lett. B **152** (1985) 256.
- [31] PYTHIA 6.3, T. Sjöstrand, L. Lönnblad, S. Mrenna and P. Skands, hep-ph/0308153.
- [32] TAUOLA 2.7, M. Jezabek, Z. Was, S. Jadach and J. H. Kühn, Comp. Phys. Commun. **64** (1991) 275.
- [33] C. Adloff *et al.* [H1 Collaboration], Eur. Phys. J. C **19** (2001) 269 [hep-ex/0012052].
- [34] T. Junk, Nucl. Instrum. Meth. A **434** (1999) 435 [hep-ex/9902006].
- [35] A. Aktas *et al.* [H1 Collaboration], Eur. Phys. J. C **33** (2004) 9 [hep-ex/0310032].



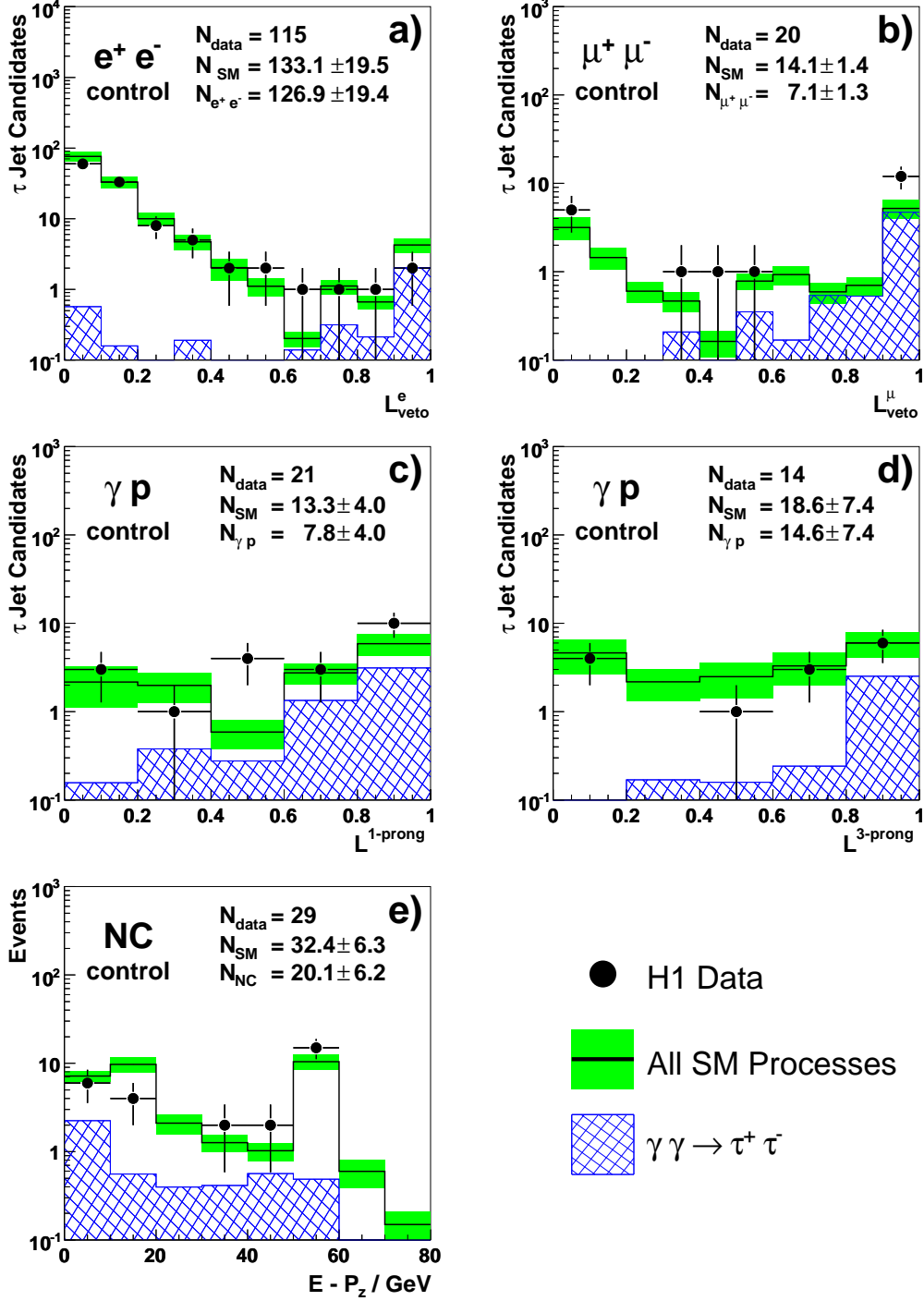


Figure 2: Distributions of **a)** the likelihood  $L_{\text{veto}}^e$  for  $\tau$ -jet candidates in the  $\gamma\gamma \rightarrow e^+e^-$  control sample, **b)** the likelihood  $L_{\text{veto}}^\mu$  for  $\tau$ -jet candidates in the  $\gamma\gamma \rightarrow \mu^+\mu^-$  control sample, **c)** and **d)** the NN outputs  $L^{1\text{-prong}}$  and  $L^{3\text{-prong}}$  for 1-prong and 3-prong  $\tau$ -jet candidates in the  $\gamma p$  control sample, and **e)** the longitudinal momentum balance  $E - P_z$  in the NC DIS control sample. In each figure the open histogram shows the total SM expectation and the shaded band its uncertainty. The contribution from tau pair production is shown as the hatched histogram.

# H1

## TAU PAIR CANDIDATE

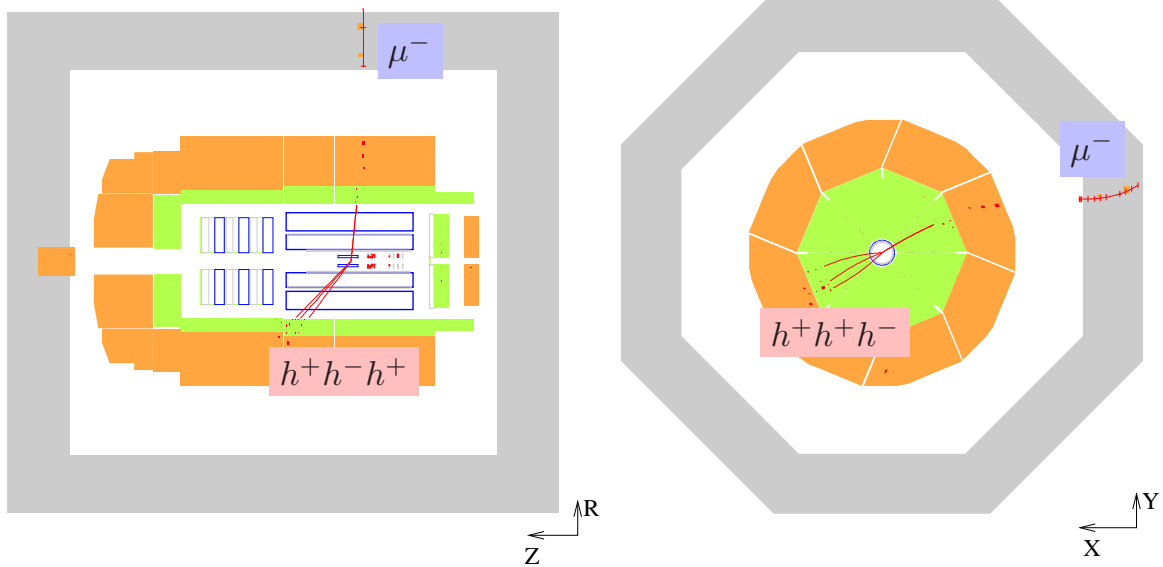
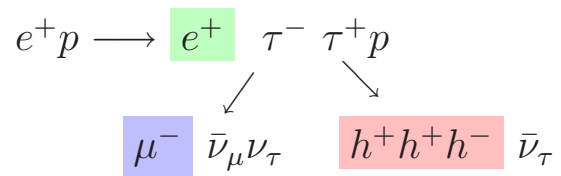


Figure 3: A tau pair candidate event with one tau lepton decaying leptonically to a muon and the other tau lepton decaying to three charged hadrons (3-prong topology).

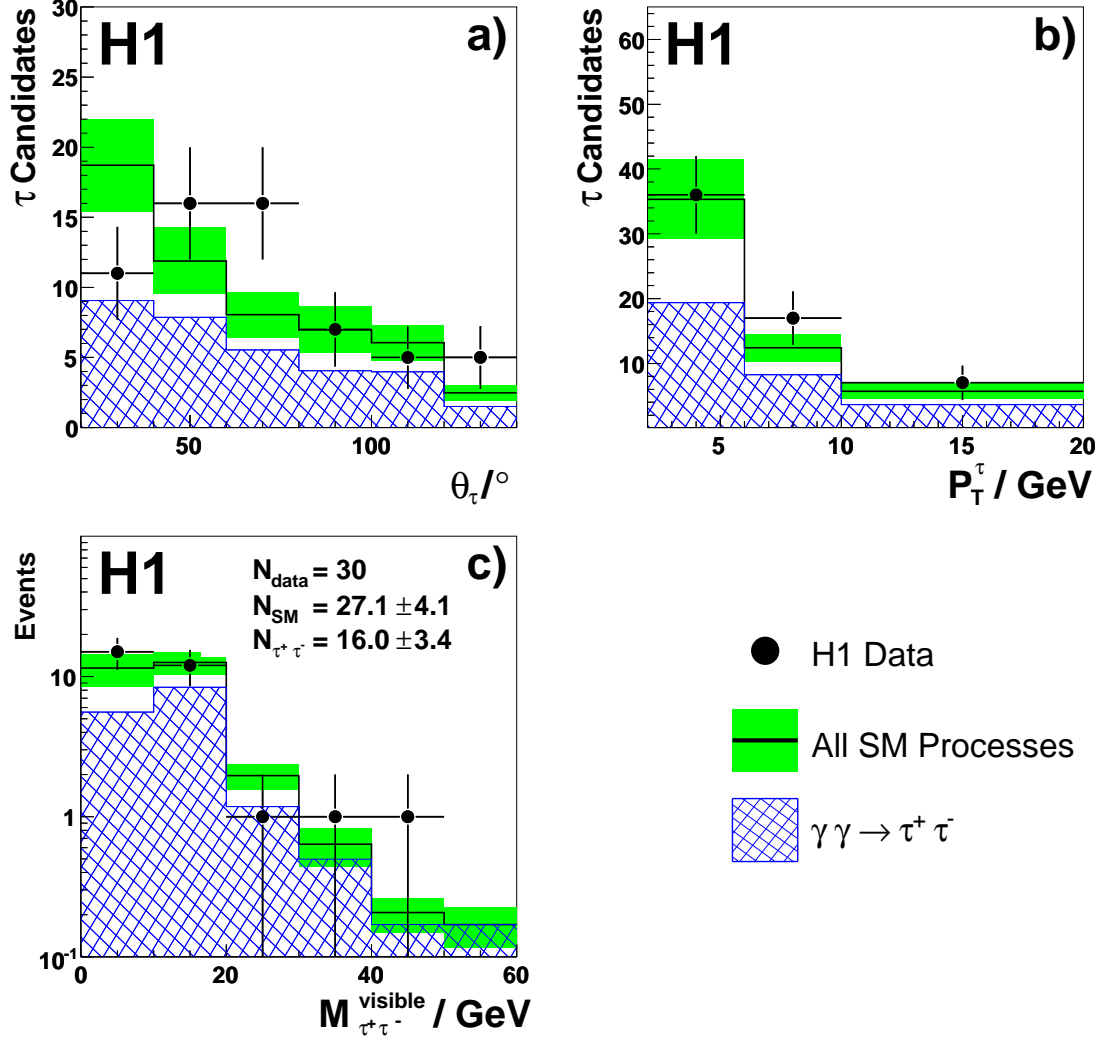


Figure 4: Distributions of **a)** the polar angle and **b)** the transverse momentum of the reconstructed  $\tau$  lepton candidates in the  $\tau^+\tau^-$  event sample. The invariant mass of the tau candidate pair is shown in **c)**. The selected events enter distributions **a)** and **b)** twice. In each figure the open histogram shows the total SM expectation and the shaded band its uncertainty. The contribution from tau pair production is shown as the hatched histogram.

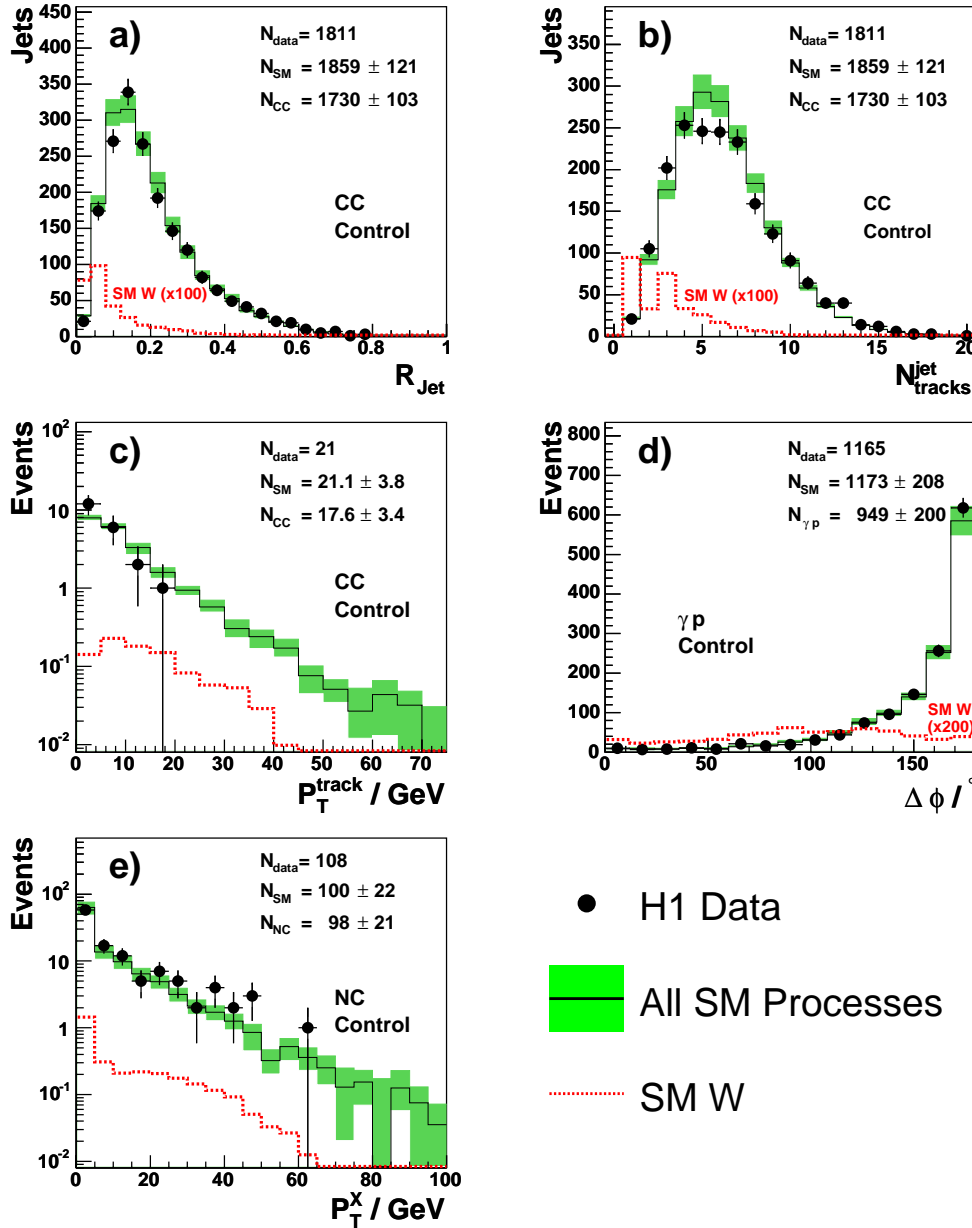


Figure 5: Control distributions in the background enriched samples defined for the  $\tau + P_T^{\text{miss}}$  analysis: **a)** the radius of isolated jets, **b)** the number of charged particles in each isolated jet and **c)** the transverse momentum of the track associated to single track isolated jets in the CC DIS control sample; **d)** the acoplanarity angle between the isolated jet and the remaining hadronic system X in the  $\gamma p$  control sample; **e)** the transverse momentum of the hadronic system X excluding the isolated jet candidate in the NC DIS control sample. In all distributions each event may enter several times, depending on the number of isolated jets in the event. In each figure the data (points) are compared to the SM expectation (solid histogram) shown with its uncertainty (shaded band). The signal contribution dominated by the SM W production is also shown (dashed histogram). In **a)** and **b)** it is shown multiplied by a factor 100 and in **d)** by 200.

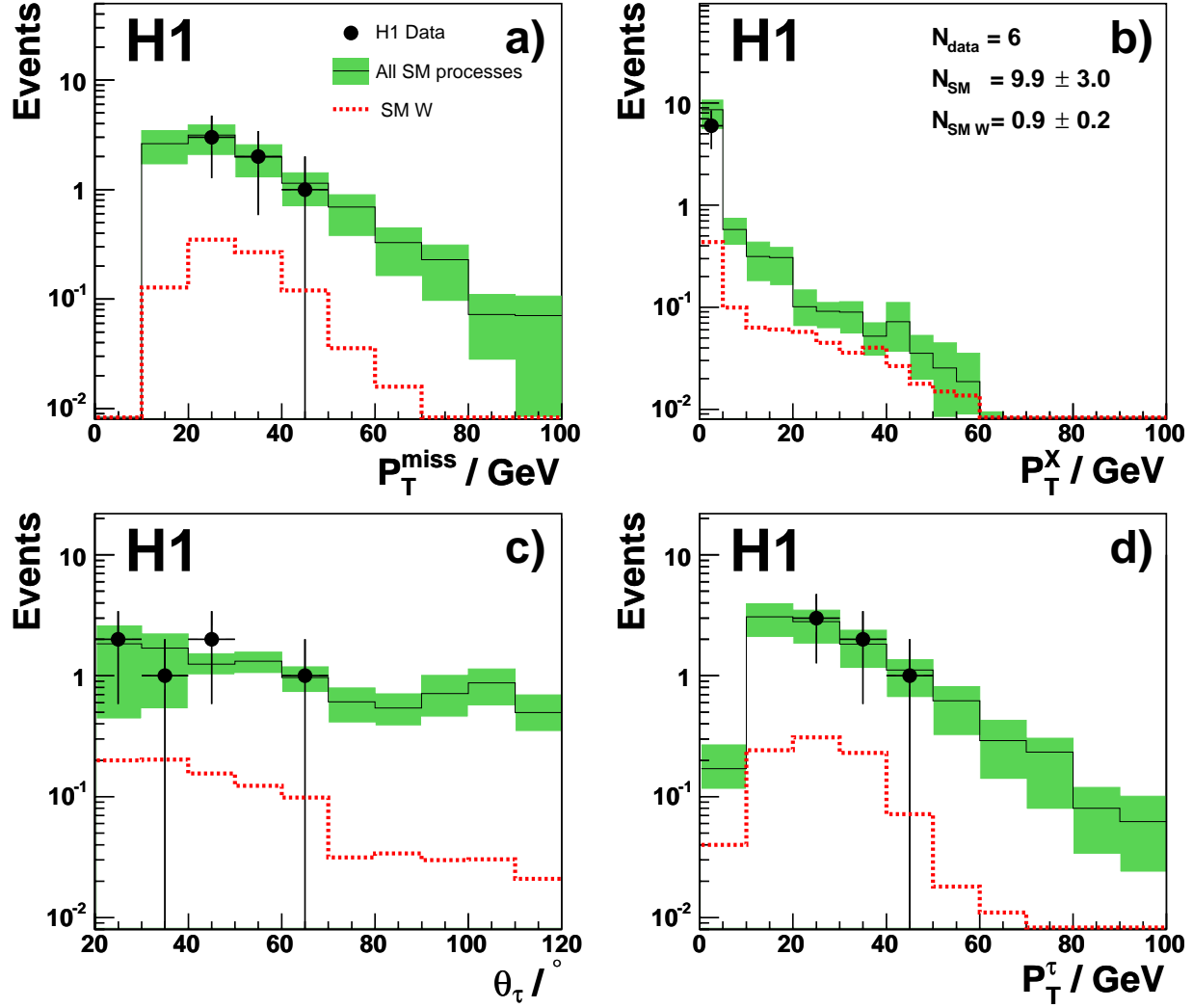


Figure 6: Distributions of **a)** the total missing transverse momentum  $P_T^{\text{miss}}$ , **b)** the hadronic transverse momentum  $P_T^X$ , **c)** the polar angle  $\theta_\tau$  and **d)** the transverse momentum  $P_T^\tau$  of the  $\tau$ -jet candidate in the final sample of events containing an isolated tau lepton and large missing transverse momentum. In each figure the data (points) are compared to the SM expectation (solid histogram) shown with its uncertainty (shaded band). The signal contribution dominated by the SM  $W$  production is also shown (dashed histogram).